Late Holocene variability in Florida Current surface density: Patterns and possible causes

D. C. Lund

Massachusetts Institute of Technology/Woods Hole Oceanographic Institution Joint Program in Oceanography, Woods Hole Oceanographic Institution, Woods Hole, Massachusetts, USA

W. B. Curry

Department of Geology and Geophysics, Woods Hole Oceanographic Institution, Woods Hole, Massachusetts, USA

Received 14 January 2004; revised 28 May 2004; accepted 16 July 2004; published 5 October 2004.

[1] Planktonic foraminiferal $\delta^{18}O$ time series from three well-dated, high sedimentation rate cores near the Florida Keys (24.4°N, 83.3°W) exhibit repeated centennial to millennial-scale oscillations during the late Holocene. Isotopic shifts of 0.2–0.3‰ over the past 5200 years represent changes in sea-surface temperature (SST) of 1.0–1.5°C or salinity variability of 1–2 psu. The largest significant isotopic events are centered at approximately 200, 2000, 3200, and prior to 4000 calendar years BP. High Florida Current $\delta^{18}O$ during the Little Ice Age (LIA) correlates with published records of high $\delta^{18}O$ in the Sargasso Sea and low SST off the coast of west Africa. An interval of generally low $\delta^{18}O$ in the Florida Straits from 1800 to 500 years BP is synchronous with the Medieval Warm Period off west Africa but leads low $\delta^{18}O$ in the Sargasso Sea by several hundred years. Synchronous cooling across the subtropical gyre during the LIA is difficult to explain using interannual North Atlantic Oscillation patterns but may be consistent with the simulated effects of reduced solar irradiance. At frequencies between 1/1000 and 1/300 years during the Late Holocene, Florida Current $\delta^{18}O$ is coherent with a published estimate of ^{14}C production rate. Radiocarbon production seems to lead $\delta^{18}O$ at these frequencies, but uncertainty in the phase calculation precludes a clear lead-lag relationship. At frequencies lower than 1/300 years, Florida Current $\delta^{18}O$ is coherent and in phase with atmospheric $\Delta^{14}C$. The coherence of $\Delta^{14}C$ and $\delta^{18}O$ at periods >1000 years implies oceanic circulation may play a role in modulating atmospheric radiocarbon on millennial timescales. *INDEX TERMS:* 4215 Oceanography: General: Climate and interannual variability (3309); 4576 Oceanography: Physical: Western boundary currents; 4870 Oceanography: Biological and Chemical: Stable isotopes; *KEYWORDS:* Holocene, Florida current, density

Citation: Lund, D. C., and W. B. Curry (2004), Late Holocene variability in Florida Current surface density: Patterns and possible causes, *Paleoceanography*, *19*, PA4001, doi:10.1029/2004PA001008.

1. Introduction

[2] The Florida Current, the portion of the Gulf Stream confined to the Straits of Florida, is a key component of the North Atlantic circulation. The flow of the Florida Current (FC) reflects both wind-driven processes in the subtropical gyre and the surface compensating flow for North Atlantic Deep Water formation. The FC transports approximately 1.3 PW (1 PW = 10^{15} W) of heat across 24.5°N [*Larsen et al.*, 1992; *Ganachaud and Wunsch*, 2000] and therefore plays a key role in regulating the climate of the circum-North Atlantic region. While the Florida Current-Gulf Stream system is arguably one of the most studied features in modern oceanography, almost nothing is known about its behavior on centennial to millennial timescales. Observations are largely limited to sea surface temperature or snapshot flow estimates during the 20th century.

[3] Here we present evidence for long-term variability in the surface density of the Florida Current over the past 5200 years using the $\delta^{18}O$ of planktonic foraminifera. Stable isotopic data from three cores indicate the surface FC was denser (colder, saltier or both) during the Little Ice Age than either the Medieval Warm Period or today. The lowest $\delta^{18}O$ values in the Florida Current during the last 5200 years occurred from 2300 to 4000 years BP, significantly lower than either core top or $\delta^{18}O_{calcite}$ calculated using modern surface temperature and salinity observations. When considered with other published results [*Keigwin*, 1996; *deMenocal et al.*, 2000], it is possible that the entire subtropical gyre of the North Atlantic cooled during the Little Ice Age, a pattern unlike the interannual variations in the North Atlantic Oscillation [*deMenocal et al.*, 2000], but perhaps consistent with the simulated effects of reduced solar irradiance [*Rind and Overpeck*, 1993; *Shindell et al.*, 2001].

2. Background

2.1. Modern Oceanographic Setting

[4] The Florida Current, with an annual average flow of 31 Sv (1 Sv = 10^6 m^3 s^{-1}), is composed of two primary

0883-8305/04/2004PA001008$12.00

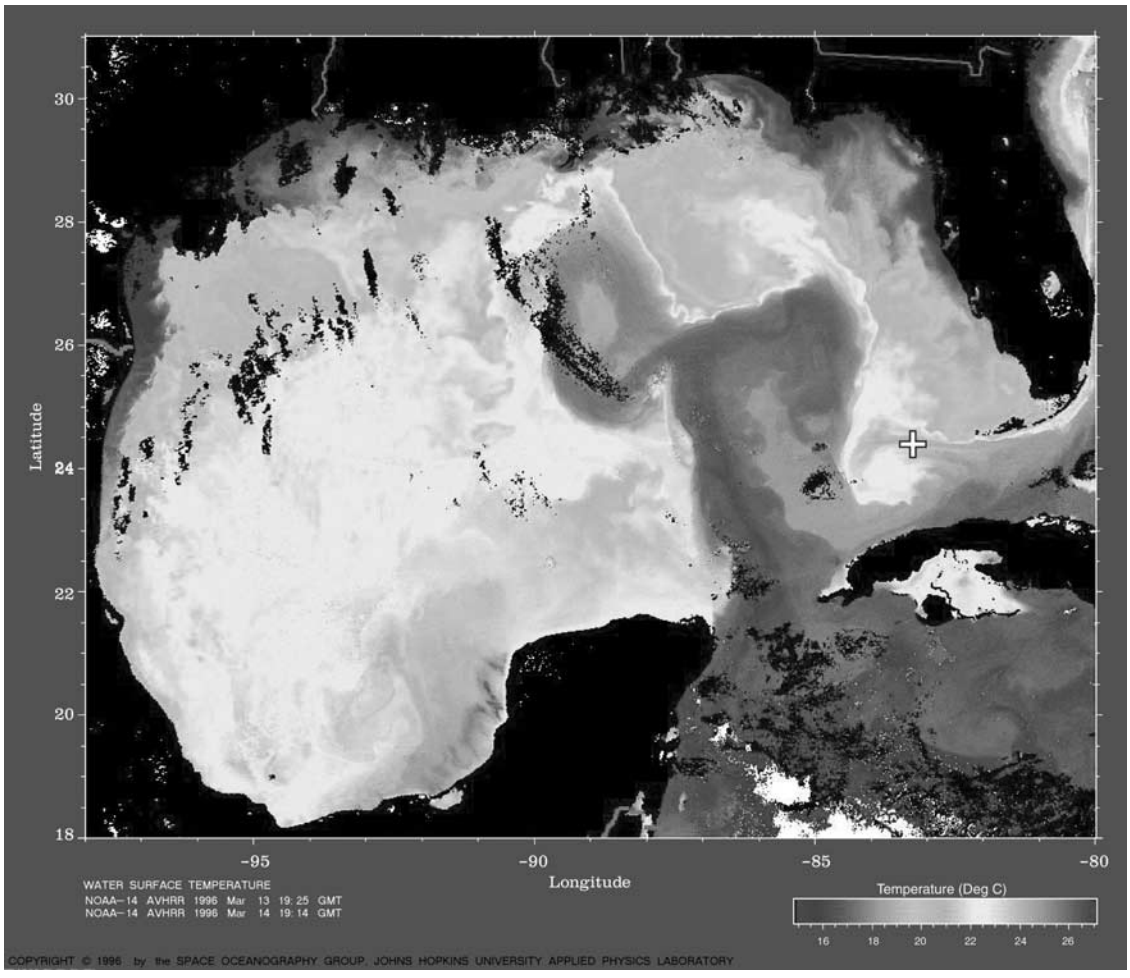

Figure 1. Advanced very high resolution radiometer (AVHRR)-based sea surface temperature estimates for the Gulf of Mexico and Florida Straits, 13–14 March 1996. SSTs in this figure vary from 15 to 27°C. The strong north-south temperature gradient near the core sites (plus symbol) is typical of winter conditions in this area (reprinted by permission from Ocean Remote Sensing Group, Johns Hopkins University Applied Physics Laboratory). See color version of this figure at back of this issue.

components; one from the wind-driven subtropical gyre (17 Sv) and the other from the tropical South Atlantic (14 Sv) [*Schmitz and Richardson*, 1991]. The fresh South Atlantic portion (<36 psu) accounts for the majority of the warmest water at the surface and coldest water near the bottom of the Florida Current (FC). In between these two components flows high salinity (>36 psu) water of the North Atlantic subtropical gyre [*Schmitz et al.*, 1993]. The estimate of the South Atlantic contribution is similar to the formation rate of North Atlantic Deep Water (13–14 Sv) implying that the South Atlantic portion of the FC compensates NADW formation [*Schmitz and McCartney*, 1993].

[5] The transport of the Florida Current varies on annual and interannual timescales. The best time series of FC variability are transport estimates based on the voltage difference in submarine telephone cables across the Straits of Florida. Using 16 years of data, *Baringer and Larsen* [2001] calculated an annual minimum of 30 Sv in January and maximum of 34 Sv in July. Decadal variations in FC transport of ±2 Sv seem to be negatively correlated with the NAO index, but the link between the two remains unclear due the limited length of the observations [*Baringer and Larsen*, 2001].

[6] Climatological sea surface temperatures at the coring sites discussed in this paper (near Dry Tortugas: ~24.5°N, 83.5°W) range from a summer maximum of approximately 30°C to a winter minimum of 24°C [*Levitus et al.*, 1994]. Satellite imagery indicates the presence of a strong meridional temperature gradient in this region from September through April, due to the juxtaposition of warm Florida Current water and colder water along the West Florida Shelf. An advanced very high resolution radiometer (AVHRR)-based SST map from mid-March 1996 shows the Loop Current penetrating into the Gulf of Mexico, then returning southward and eventually eastward into the Florida Straits (Figure 1). Northward incursions of the Loop Current and shedding of a large anticyclonic ring occurs on an aperiodic basis [*Vukovich*, 1988; *Sturges and Leben*, 2000].

[7] When the Loop Current is fully developed, frontal eddies propagated along its outer boundary generate cyclonic mesoscale features near Dry Tortugas [*Fratantoni et al.*, 1998]. The so-called Tortugas eddies persist on the order of 100 days and are eventually dislodged and taken downstream by meanders in the Florida Current [*Lee et al.*, 1995; *Fratantoni et al.*, 1998]. The presence of these eddies tends to cool SSTs near Dry Tortugas, except in the summer months when SSTs in the Gulf of Mexico and Florida Current are nearly homogeneous [*Levitus et al.*, 1994].

2.2. Little Ice Age Record

[8] The majority of our knowledge of the Little Ice Age comes from land-based historical and paleoclimate records. Historical accounts describe severe cold conditions in Europe and North America at intermittent periods during the LIA [*Grove*, 1988; *Jones and Bradley*, 1995]. Terrestrial paleoclimatic records, including Northern Hemisphere tree ring-based temperature reconstructions [*Bradley and Jones*, 1993; *Mann et al.*, 1999; *Esper et al.*, 2002], borehole temperature estimates [*Dahl-Jensen et al.*, 1998; *Huang et al.*, 2000], inferred temperatures from tropical and subtropical ice cores [*Thompson*, 1995], and glacial moraines in North America [*Denton and Karlén*, 1973] and New Zealand [*Chinn*, 1996] indicate the LIA was a hemispheric and perhaps global phenomenon.

[9] Several lines of evidence from marine sediments and coral records show that the surface North Atlantic was subject to centennial- and millennial-scale climate variability during the late Holocene culminating in the widespread effects of the Little Ice Age. Using planktonic foraminiferal $\delta^{18}O$, *Keigwin* [1996] estimated that SSTs in the Sargasso Sea during the Little Ice Age (LIA; ~50–450 years BP) were ~1°C cooler than today, while SSTs at 1000 years BP were ~1°C warmer. In the eastern part of the subtropical gyre, *deMenocal et al.* [2000] found a cooling of nearly 4°C during the LIA using foraminiferal-based faunal estimates of SST. In both locations, the LIA is preceded by relatively a warm interval, or so-called ''medieval Warm Period'' from roughly 700 to 1500 BP. The larger SST response in the eastern gyre is likely due to its proximity to the west African coast and greater sensitivity to wind-driven changes in upwelling. At the western edge of the gyre, corals from the Florida Keys and Puerto Rico experienced cooling of 1–3°C relative to today during the coldest intervals of the LIA [*Druffel*, 1982; *Winter et al.*, 2000].

[10] In the subpolar North Atlantic the pattern is more complicated. While *Keigwin and Pickart* [1999] have shown that LIA sediments south of Newfoundland contained lower concentrations of left coiling *N. pachyderma*, which would indicate local warming, *Bond et al.* [2001] observed increased flux of ice rafted debris (IRD) and the presence of colder-water fossils in the subpolar North Atlantic, consistent with generally colder conditions. *Keigwin and Pickart* [1999] likened the LIA to a prolonged negative phase of the NAO, but *deMenocal et al.* [2000] noted that cooling across the subtropical gyre during the LIA is unlike the NAO pattern. *Bond et al.* [2001] argued that episodic IRD events and cooling in the North Atlantic are tied to changes in the production rate of atmospheric ^{14}C and ^{10}Be, and proposed a link between solar irradiance, ocean circulation and climate on millennial timescales.

[11] Despite abundant historical and paleoclimatic evidence, there remain substantial gaps in our knowledge of the magnitude, timing, and spatial patterns of observed temperature anomalies during the late Holocene. As a result, there is no consensus on the mechanisms of climate change during this time. Fluctuations in solar output [*Eddy*, 1976; *Lean and Rind*, 1999; *Bond et al.*, 2001], volcanic activity [*Crowley*, 2000], North Atlantic Deep Water formation [*Bianchi and McCave*, 1999; *Keigwin and Boyle*, 2000; *Bond et al.*, 2001; *Oppo et al.*, 2003], the frequency of the El Niño Southern Oscillation [*Haug et al.*, 2001; *Cobb et al.*, 2003] and the North Atlantic Oscillation [*Keigwin*, 1996; *Keigwin and Pickart*, 1999], are all cited as possible causes of or contributors to Holocene climate variability. In this paper, our aim is to firmly establish the pattern and timing of surface density variations in the Florida Straits during the past 5000 years. With this information in hand, we hope to determine whether variations in NADW formation or shifts in NAO phase, two mechanisms that directly influence the Florida Current, may have contributed to events such as the Little Ice Age.

3. Methods and Materials

[12] The three sediment cores used for this study, W167-79GGC (530 m depth; 24°21.5′N, 83°20.9′W), KNR166-2-62MC-A (547 m depth; 24°19.6′N, 83°15.4′W), and C166A-8GGC (435 m depth; 24°23.1′N, 83°20.3′W) were raised from the Florida continental slope in an area of high sediment accumulation south of Dry Tortugas (Figure 1). Core samples were taken at intervals of 0.5 cm for 79GGC, 0.5 cm for 62MC, and 2 cm for 8GGC, equivalent to an average sample spacing of 21, 16, and 35 years, respectively (see next section). Planktonic foraminifera are abundant in each core, allowing for multiple replicate measurements at each stratigraphic level. For a typical sample, we used 10 *G. ruber* tests (white; 212–250 μm size fraction) per stable isotopic analysis, and measured four replicate analyses at each depth. Prior to analysis, we briefly sonicated each sample in methanol to remove detrital material from the foraminiferal shells.

[13] Isotopic samples from 79GGC and 8GGC were analyzed using a Finnigan MAT 252 coupled to a Kiel II automated carbonate device following the procedure outlined in the work of *Ostermann and Curry* [2000]. Calibration to VPDB scale was made using NBS-19 ($\delta^{18}O$ = −2.20‰ and $\delta^{13}C$ = 1.95‰). Long-term reproducibility (1σ) of NBS-19 (n > 2200) for this mass spectrometer system is ±0.07‰ for $\delta^{18}O$ and ±0.03‰ for $\delta^{13}C$ [*Ostermann and Curry*, 2000]. Samples from 62MC were run on a new Finnigan MAT 253 coupled to a Kiel III carbonate device. Replicate analyses of NBS-19 (n = 133) on this mass spectrometer yield a comparable analytical precision of ±0.08‰ for $\delta^{18}O$ and ±0.02‰ for $\delta^{13}C$.

4. Age Models

[14] The age model for W167-79GGC is based on 14 radiocarbon dates, the age model for C166A-8GGC has

Table 1. Radiocarbon Ages for W167-79GGC, C166A-8GGC, and KNR166-2-62MC-A[a]

Depth Range, cm	^{14}C Age, years	Error, years	Calendar Age, years BP	Model Age, years	Species
		W167-79GGC			
0–1	765	95	424	N/A	*G. sacculifer*
0–1	350	40	0	0	*G. ruber*
4–5	440	35	40	N/A	*G. sacculifer*
8–9	995	30	560	560	*G. sacculifer*
20–21	1270	25	796	796	*G. sacculifer*
31–31.5	1730	45	1278	1278	*G. sacculifer*
40.5–41	1870	30	1403	1403	*G. sacculifer*
54.5–55	2560	35	2272	2272	*G. sacculifer*
69–70	2800	35	2530	2530	*G. sacculifer*
84–84.5	3010	30	2759	2759	*G. sacculifer*
99–100	3470	30	3348	3348	*G. sacculifer*
114–115	4190	40	4266	4266	*G. sacculifer*
127–128	4810	45	5049	5210	*G. ruber*
127–128	5030	50	5371	5210	*G. sacculifer*
		C166A-8GGC			
0–1	155	30	0	0	*G. ruber*
1.5–2.5	465	40	60	60	*G. sacculifer*
26.5–27.5	795	35	447	504	*G. ruber*
26.5–27.5	995	35	560	504	*G. sacculifer*
38.5–39.5	1810	40	1338	N/A	*G. ruber*
38.5–39.5	1390	35	928	928	*G. sacculifer*
58.5–59.5	1690	120	1254	1254	*G. ruber*
58.5–59.5	1130	35	667	N/A	*G. sacculifer*
96.5–97.5	2370	40	1984	1913	*G. ruber*
96.5–97.5	2240	60	1842	1913	*G. sacculifer*
150.5–151.5	2920	35	2713	2849	*G. ruber*
150.5–151.5	3200	40	2985	2849	*G. sacculifer*
		KNR166-2-62MC-A			
0–1	>mod	N/A	post-1950 A.D.	0	*G. ruber*
29–29.5	1420	35	955	955	*G. ruber*

[a]We converted our raw ^{14}C values to calendar ages using CALIB 4.3 [*Stuiver et al.*, 1998] and a reservoir age of 400 years. See text for age model construction details.

12, and KNR166-2-62MC-A has two (see Table 1). The dates are based on either *Globigerinoides sacculifer* or *Globigerinoides ruber* from the >250 μm size fraction. In each case, the raw radiocarbon values were corrected for a 400-year reservoir effect and then converted to calendar ages using CALIB 4.3 [*Stuiver et al.*, 1998]. In some cases, analyses of *G. ruber* and *G. sacculifer* in the same core and at the same depth reveal age offsets of up to several hundred years, with no consistent pattern. For the gravity cores, we used the *G. ruber* values for the core top datum since the raw ^{14}C values of <400 years imply the presence of radiocarbon from nuclear testing, and hence a near-modern age. For the multicore 62MC the fraction of modern ^{14}C in the core top exceeds one, indicating an age younger than 1950 A.D. For each of the cores discussed here, the core top calendar age is assumed to be 0 cal (calendar) years BP, but this assumption is strongest for 62MC.

[15] Down core age control points in 79GGC are based on the *G. sacculifer* values, except the core bottom age, which is an average from both *G. sacculifer* and *G. ruber*. We omitted a ^{14}C measurement at 4.5 cm from the age model as it would require a sedimentation rate of >110 cm kyr^{-1} near the core top, an unrealistic value considering the average sedimentation rate of ~24 cm kyr^{-1} for 79GGC. Down core values for 8GGC at 27, 97, and 151 cm are two-species averages. The age control points for 8GGC are less certain at 39 and 59 cm, given the apparent age reversal in this range. Here we chose dates most consistent with the average sedimentation rate (53 cm kyr^{-1}); 928 years at 39 cm (*G. sacculifer*) and 1254 years at 59 cm (*G. ruber*).

5. The $\delta^{18}O$ Results

[16] Average values of *G. ruber* $\delta^{18}O$ at each stratigraphic depth reveal long-term trends in surface density in the three cores. In 79GGC, $\delta^{18}O$ values are highest (coldest temperatures and/or highest salinity) at approximately 200 years BP, 2000 years BP, and prior to 4000 years BP (Figure 2a). The lowest values of the entire record occur between approximately 2500 to 3500 years before present. In 8GGC, high $\delta^{18}O$ intervals are centered at 200 and 2000 years BP (Figure 2b), at about the same timing as events in 79GGC. In 8GGC, *G. ruber* $\delta^{18}O$ is lowest from ~1000 to 1700 years BP and prior to 2700 years BP. In 62MC, the shortest of the three records, there is an interval of high $\delta^{18}O$ centered at about 200 years BP (Figure 2c), similar to the nearby gravity cores.

[17] At first glance, the scatter of *G. ruber* $\delta^{18}O$ values in each core appears to be unusually large, but much of the variance results from seasonal changes in the *G. ruber* population and our isotopic sampling and measurement strategy. Using time series of estimated monthly sea surface

temperature and climatological salinity at 24°N, 83°W [*Levitus et al.*, 1994], we calculated the seasonal $\delta^{18}O_{calcite}$ signal using a $\delta^{18}O$/SST relationship of 0.22‰/°C [*Epstein et al.*, 1953] and $\delta^{18}O$/salinity slope of 0.11‰/psu [*Fairbanks et al.*, 1992]. Since the annual changes in surface salinity are small compared to SST, the $\delta^{18}O$ variability is due primarily due to temperature. To simulate our sampling strategy, we sampled the calculated $\delta^{18}O_{calcite}$ time series randomly 10 times and took the average to simulate one $\delta^{18}O$ analysis of 10 *G. ruber* individuals. The calculated standard deviation of the resulting mean values is ±0.15‰ (σ_s, n = 10,000). Combining this with a mass spectrometer analytical error of ±0.08‰ (σ_m), we should expect a standard deviation for real measurements of ±0.17‰ ($\sigma^2 = \sigma_s^2 + \sigma_m^2$; *Killingley et al.* [1981]).

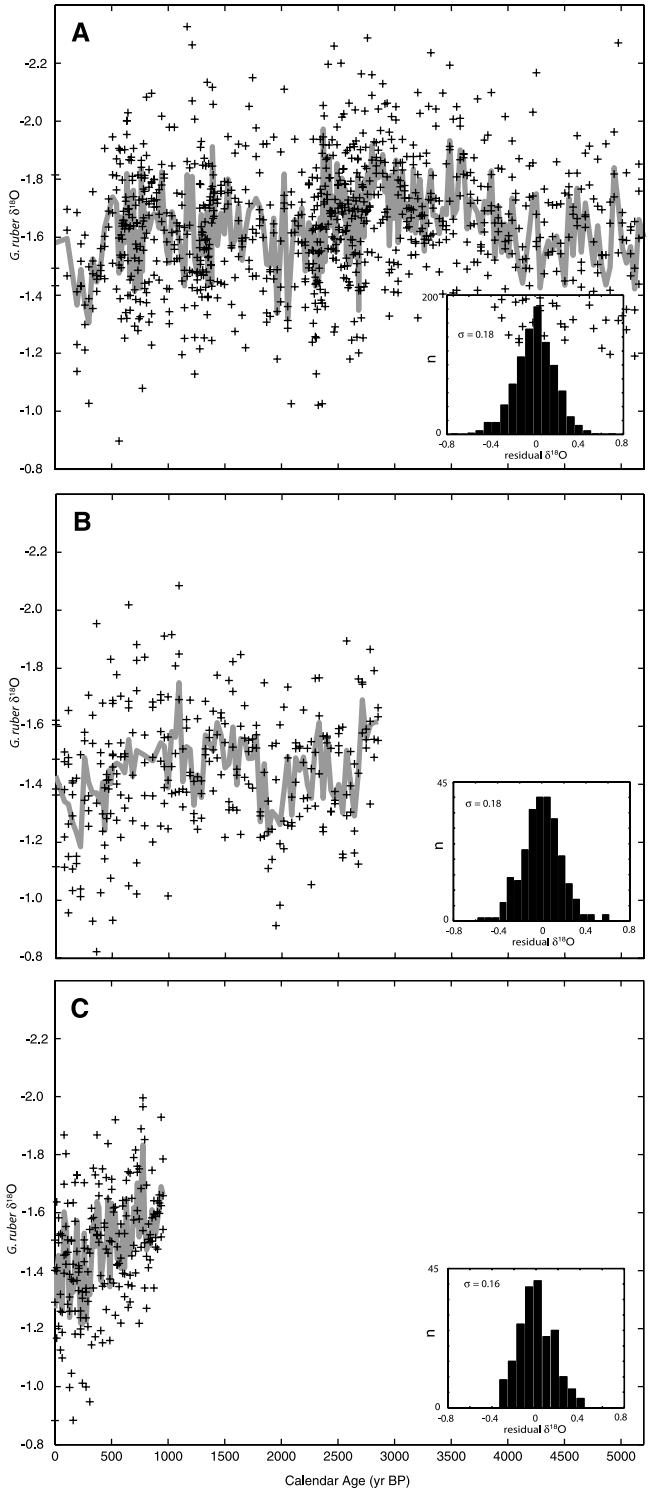

Figure 2. (a) Individual *G. ruber* $\delta^{18}O$ analyses for 79GGC (pluses) and average values at each depth (gray line). Intervals of heavy average $\delta^{18}O$ occur at approximately 200 years BP, 2000 years BP, and prior to 4000 years BP. Inset is the histogram for residual $\delta^{18}O$ values; residuals were calculated by subtracting the mean value at each depth from each $\delta^{18}O$ analysis. The distribution is approximately normal with a standard deviation of 0.18‰. (b) Same as previous, except for 8GGC. Intervals of heavy $\delta^{18}O$ occur at approximately 200 and 2000 years BP. Note the smaller number of samples relative to 79GGC and that mean $\delta^{18}O$ for 8GGC is ~0.2‰ heavier than for 79GGC. The standard deviation of $\delta^{18}O$ residuals is equal in the two cores. (c) Same as previous, except for 62MC. The highest average $\delta^{18}O$ occurred at approximately 200 years BP. The standard deviation of 0.16‰ for residual values is similar to that in 8GGC and 79GGC.

[18] The expected variance is almost identical to the values we observe: for 79GGC and 8GGC the 1σ standard deviation of residual $\delta^{18}O$ values is 0.18‰ (Figures 2a and 2b), while for 62MC the 1σ standard deviation of residuals is 0.16‰ (Figure 2c). We used residual values (individual $\delta^{18}O$ measurement minus the mean at each sampling depth) to ensure the calculated variance is independent of the mean climate state. In comparison to the predicted values, the variance in each core is not unusual, but what should be expected given the seasonal range in temperature and the likelihood that *G. ruber* is present at these sites year-round. Sediment trap studies [*Deuser*, 1987] and plankton tow data [*Williams et al.*, 1979] from the Sargasso Sea near Bermuda indicate year-round production of *G. ruber* (white) over an annual range of sea surface temperatures (20–28°C), comparable to that observed at our core sites in the Florida Straits (24–30°C).

[19] In each core, there are several one point excursions of depth-averaged $\delta^{18}O$ in excess of 0.3‰ (Figure 2). Many of the extreme $\delta^{18}O$ values probably can be explained by a disproportionate sampling of *G. ruber* individuals that calcified during the summer or winter months. To capture the mean $\delta^{18}O$ value in a sample with a precision approaching the limitations of the mass spectrometer requires approximately 200 individual *G. ruber* specimens, either with 200 individuals in one sample or with 20 samples of 10 individuals each. We accomplish the latter by smoothing with a 100 year moving average to group samples and calculate a stable mean $\delta^{18}O$ value (Figure 3). While making multiple measurements is more labor intensive than grouping samples together for a single analysis, the larger number of analyses reduces the standard error and the width of the confidence limits for each mean value.

[20] The confidence limits allow for quantitative evaluation of the difference between $\delta^{18}O$ values in various parts

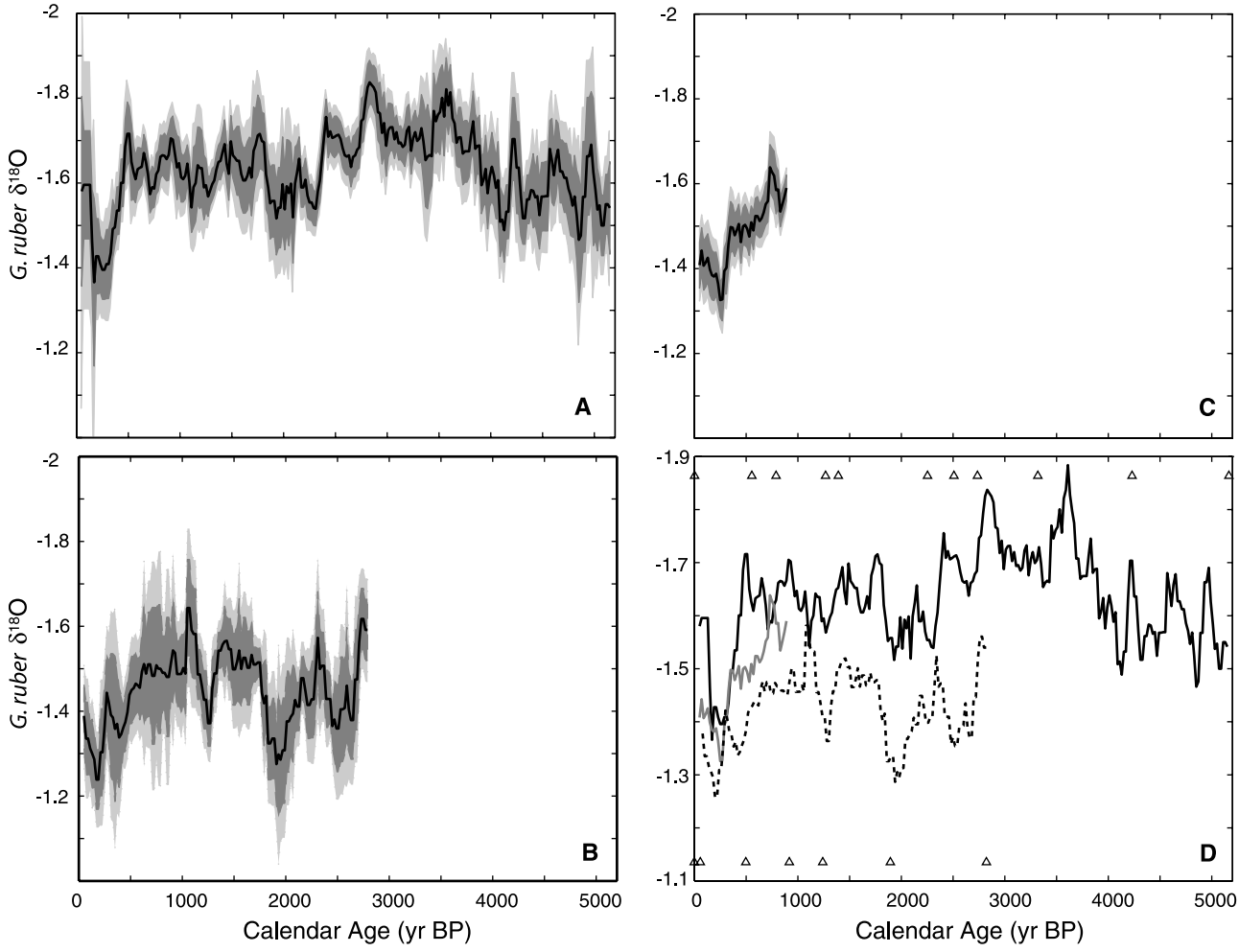

Figure 3. (a) One hundred year running mean *G. ruber* $\delta^{18}O$ for 79GGC, (b) 8GGC, and (c) 62MC. Mean values are represented by the black line. The 95% (light gray) and 80% (dark gray) confidence intervals were calculated using a t distribution. There are three periods of heavy $\delta^{18}O$ in 79GGC from ~100–400 years BP, ~1800–2300 years BP, and prior to 4000 years BP. (d) One hundred year running mean time series for all three cores (solid curve, 79 ggc; dashed curve, 8 ggc; gray curve, 62 mc). All three time series record low SST and/or high salinity conditions 200–300 years ago. Here 79GGC and 8GGC indicate an interval of high surface water density about 2000 years ago.

of the time series. For example, at 95% confidence, the mean $\delta^{18}O$ at 250 cal years BP in 79GGC is higher than the mean from ~500–1000 and 1300–1500 years BP; at 80% confidence, it is greater than any mean value between 500 and 1800 years BP (Figure 3a). Similar to the pattern indicated by the simpler depth averaging approach, there are three primary intervals of high $\delta^{18}O$ centered at 200 years BP, 2000 years BP, and prior to 4000 years BP. The 100-year moving average $\delta^{18}O$ for 8GGC is broadly similar to 79GGC, though it differs in detail. Using the 80% confidence interval as a guide, high $\delta^{18}O$ near 200 and 2000 years BP also occur in 8GGC (Figure 3b). At 95% confidence, however, the mean of the 200 years BP event is only greater than intervals from ~1000–1200, 1400–1500, and 1700–1800 years BP.

[21] The wider confidence limits in 8GGC relative 79GGC are due primarily to differences in sampling density: from 0–2850 years BP in 79GGC there are 613 $\delta^{18}O$ analyses, while in 8GGC there are 282. In contrast, the number of measurements in 62MC is comparable to the number in 79GGC from 0–1000 years BP (198 and 170, respectively). Similar to 79GGC, the $\delta^{18}O$ value at ~250 years BP in 62MC is significantly heavier than the mean $\delta^{18}O$ prior to 500 years BP, based on the 95% confidence interval (95% confidence interval (CI); Figure 3c). For both 79GGC and 62MC, the change in mean $\delta^{18}O$ from 1000 years BP to 250 years BP is 0.2–0.3‰ (95% CI). Since 250 years BP, $\delta^{18}O$ decreased 0.2‰ in 79GGC and 0.1‰ in 62MC (80% CI). In 8GGC, the $\delta^{18}O$ decrease in this time period of 0.1‰ is not significant at 80% confidence.

5.1. Surface Density Over Past 1000 Years

[22] Cores 79GGC and 62MC have high sampling density, exhibit similar changes in $\delta^{18}O$, and seem to provide a consistent picture of surface water $\delta^{18}O$ during the past 1000 years. Each core records a $\delta^{18}O$ increase of 0.2–0.3‰

from 1000 to 250 years BP, which if entirely due to temperature, is equivalent to a 1–1.5°C SST cooling. Similarly, a $\delta^{18}O$ decrease of 0.1–0.2‰ since 250 years BP may represent an SST warming of 0.5–1.0°C. If due to salinity, the $\delta^{18}O$ changes would require variability of 1–2 psu, assuming a $\delta^{18}O$/salinity relationship of 0.1–0.2‰/psu [*Fairbanks et al.*, 1992]. While on a seasonal basis salinity plays a minor role in controlling surface water $\delta^{18}O$, we cannot rule out longer term changes in salinity at these sites. Mg/Ca measurements in corals near Puerto Rico indicate that SSTs from 1987–1993 A.D. were 2 ± 1°C warmer than those from 1699–1703 A.D. [*Watanabe et al.*, 2001], similar to the temperature change estimated from Sr/Ca in sclerosponges near Jamaica [*Haase-Schramm et al.*, 2003]. This shift is larger than implied by the $\delta^{18}O$ on the Florida Margin, but the discrepancy may be due to the lower resolution and bioturbation of the sediment records. Alternatively, lower salinity in the Florida Straits during the LIA may have masked changes in SST larger than those implied by planktonic $\delta^{18}O$.

[23] Changes in surface water pH may also influence the Florida Current $\delta^{18}O$. As pH increases, the primary form of dissolved inorganic carbon (DIC) in seawater shifts from bicarbonate to carbonate ion. Given that the carbonate ion is the isotopically lighter of the two species, the oxygen isotopic composition of DIC becomes lighter with increasing pH [*Zeebe*, 1999]. Theoretical considerations [*Zeebe*, 1999] and culturing experiments for *O. universa* [*Spero et al.*, 1997] yield a slope for $\delta^{18}O$ versus $[CO_3^{2-}]$ of ~0.002‰/(μmol kg^{-1}). Planktonic $\delta^{18}O$ during the Last Glacial Maximum may have decreased by up to 0.2‰ due lower atmospheric CO_2 and increased seawater $[CO_3^{2-}]$ [*Spero et al.*, 1997]. While we cannot rule out changes in $\delta^{18}O$ due to variable alkalinity, changes in atmospheric CO_2 during the Late Holocene have been small, on the order of 10 ppm [*Indermühle et al.*, 1999]. LGM-scale changes in CO_2 have occurred, but only in the past 200 years [*Etheridge et al.*, 1996], well after the observed increase in Florida Current planktonic $\delta^{18}O$ during the Little Ice Age.

[24] Prior to the LIA, *G. ruber* $\delta^{18}O$ indicates that Florida Current surface density was lower than core top values, which for 62MC are post-1950 AD, as well as lower than values calculated from modern hydrographic measurements. We calculated the $\delta^{18}O$ of calcite precipitated in equilibrium with modern surface waters ($\delta^{18}O_c$) by first determining $\delta^{18}O$ of water ($\delta^{18}O_w$) from annual average salinity and the regional relationship between $\delta^{18}O_w$ and salinity [*Lynch-Stieglitz et al.*, 1999]. We then determined $\delta^{18}O_c$ using annual average sea surface temperature and the empirical relationship between $\delta^{18}O_c$ and SST [e.g., *Kim and O'Neil*, 1997]. The predicted value for $\delta^{18}O_c$ is −1.5‰, indistinguishable from the core top values of −1.4 ± 0.1‰ (62MC), −1.6 ± 0.3‰ (79GGC) and −1.4 ± 0.2‰ (8GGC) (Figure 3). Of the three cores, the multicore provides the best estimate of modern $\delta^{18}O$, given its post-1950 A.D. core top age and relatively small uncertainty.

[25] *G. ruber* $\delta^{18}O$ is offset from equilibrium $\delta^{18}O_c$ by approximately −0.2‰ [*Fairbanks et al.*, 1982; *Curry et al.*, 1983; *Deuser*, 1987]. If we add 0.2‰ to the data to reflect this disequilibrium, then the core top value for 62MC would be 0.3‰ greater than $\delta^{18}O_c$ determined using modern hydrographic observations. Six years of sediment trap data from the Sargasso Sea indicate that seasonal changes in shell flux have little effect on annual average *G. ruber* $\delta^{18}O$ [*Deuser*, 1987], so the difference between the core top value and modern hydrography is unlikely to be caused by seasonal differences in productivity. If the seasonal pattern of *G. ruber* flux in the Florida Straits is similar to the Sargasso Sea, then the core top values may reflect real temperature and salinity differences from modern observations.

[26] Bioturbation makes the comparison of core top values to modern data difficult, but down core planktonic $\delta^{18}O$ can be evaluated relative to the 62MC core top. *G. ruber* $\delta^{18}O$ implies that hydrographic conditions at the location of 62MC prior to 500 years BP were warmer or less salty than post-1950 A. D. *G. ruber* ^{18}O in 79GGC from 500 to 2000 years BP (−1.65‰) and 2800 to 3500 years BP (−1.75‰) are also depleted relative to the 62MC core top value. This may reflect the SST gradients in this region as opposed to variations in $\delta^{18}O$ with time, however. Over the past 1000 years, the average 62MC $\delta^{18}O$ value is −1.45‰, compared to −1.55‰ for 79GGC.

5.2. Differences Between 8GGC and 79GGC

[27] Although down core variations in 79GGC and 8GGC mean $\delta^{18}O$ are similar, the absolute values in 8GGC are on average 0.15‰ greater than in 79GGC (Figure 3d). We believe the most likely explanation for this difference is the SST gradient between the coring sites. Maps of satellite-based SST estimates show a steep meridional SST gradient in this region during fall, winter, and spring, with temperature shifts of up to 5°C over only a few kilometers (Figure 1). Core 8GGC, located approximately 3 km north of 79GGC, likely has heavier $\delta^{18}O$ because it tends to experience cooler SSTs. The offset between 8GGC and 79GGC may have changed over the past 3000 years, but this difference is highly sensitive to uncertainty in the age model for each core.

5.3. Spectral Characteristics

[28] While the 79GGC and 8GGC $\delta^{18}O$ time series are similar to the eye, they are quite different in the frequency domain. We analyzed the depth-averaged (unsmoothed) $\delta^{18}O$ data (Figure 2) using multitaper spectral analysis [*Thomson*, 1982]. Each time series was linearly detrended and then interpolated using a constant sampling interval consistent with the mean time resolution of our $\delta^{18}O$ records (20 years for 79GGC and 35 years for 8GGC). The resulting spectral estimates were combined using the adaptive weighting scheme proposed by *Thomson* [1982]. A simple averaging of the spectra produces a similar result. The multitaper spectrum for 79GGC (Figure 4a) suggests periodic components in *G. ruber* $\delta^{18}O$ near 360, 190, 130, 100, and 80 years. In 8GGC, there appears to be a spectral peak at 130 years (Figure 4c). In both cores, similar features were observed using a hamming data taper and periodogram.

[29] The results of spectral analysis for any given core are highly sensitive to the age model employed. This is

particularly true for centennial-scale variability since age model errors are similar in magnitude to the derived periodic components. To test the robustness of the spectra, we created alternate age models for 8GGC and 79GGC using cubic spline rather than linear interpolation. In each case, the age model was forced to pass through the same radiocarbon control points, but abrupt changes in sedimentation rate were minimized by the spline model. While this option is not necessarily an improvement over the linear interpolation approach, it is equally plausible and demonstrates how age model uncertainty can affect the power spectrum.

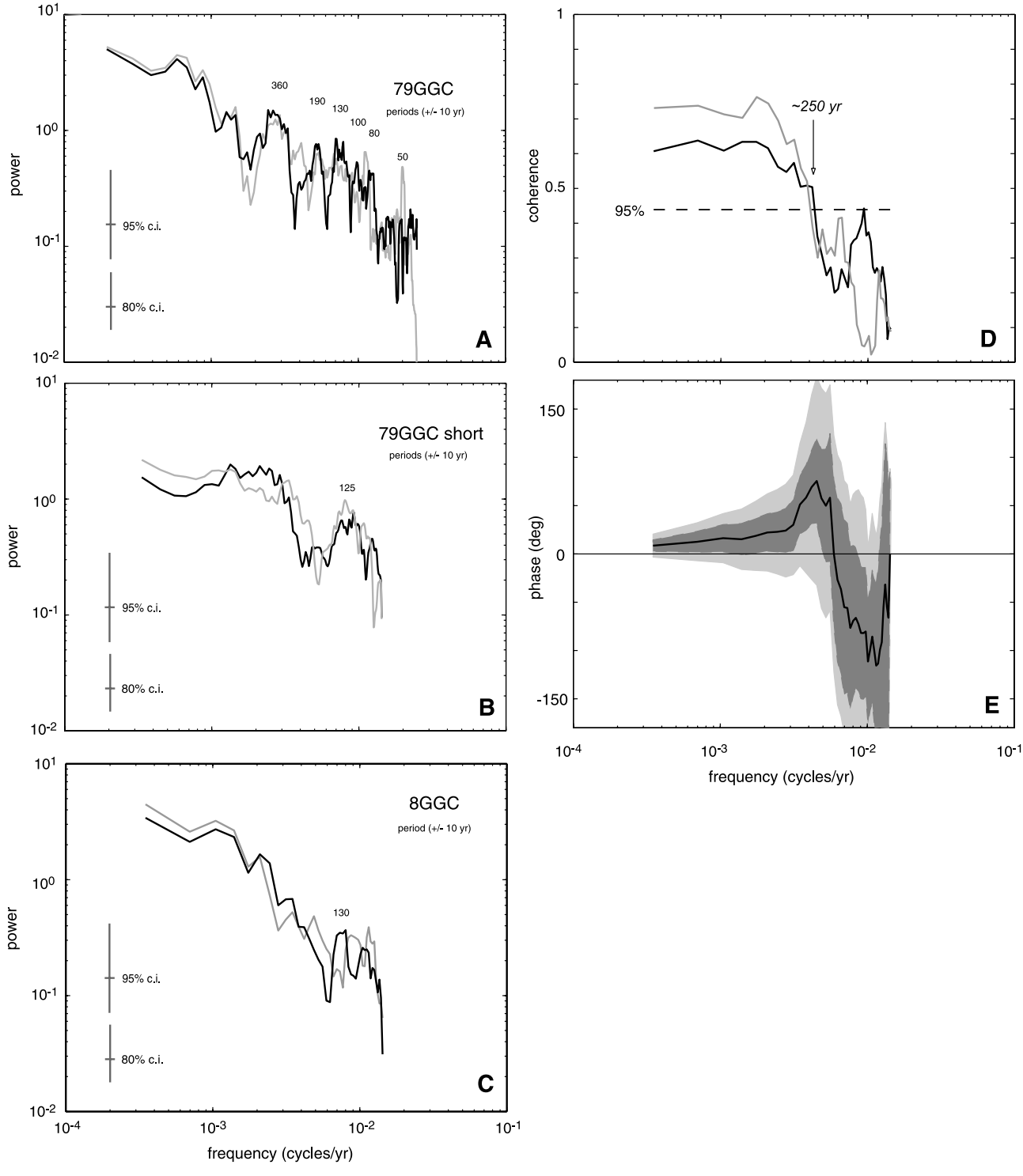

Figure 4

[30] On centennial timescales, the power spectra for the spline-based time series differ from those based on linear interpolation age models. The alternative 79GGC spectrum has peaks at periods of 360, 90, and 50 years (Figure 4a, gray curve). While there is power near 190 and 130 years, at neither period does it exceed the 95% confidence limit. The alternative spectrum for 8GGC appears to have one peak near 1/110 years, but it is not significant at the 80% level (Figure 4c). Only power at 1/360 years in 79GGC is a robust feature and it may represent a true periodic component in late Holocene planktonic $\delta^{18}O$ at this location. A complete analysis of the effects of dating uncertainty on spectral components would also take into account error in the ^{14}C control points. As such, the spline-based example given here provides a relatively optimistic view of spectral variability due to age model uncertainty.

[31] The interval from 0–2850 years in 79GGC has different spectral properties than the entire 5200-year record (Figure 4b). For both the linear and spline age models, there is a concentration of power at ~1/125 years and a broad peak between 1/1000 and 1/250 years. Cores 79GGC and 8GGC display coherent behavior at frequencies lower than ~1/250 years (Figure 4d). Nearly 35% of the coherence estimates exceed the 95% confidence level, all at low frequencies. Since neither core on its own exhibits obvious low-frequency periodic behavior, the coherence is a function of nonperiodic components in each time series. A similar result is found for the spline-based approach. Uncertainty in the radiocarbon-based chronologies and aliasing of the seasonal SST cycle make it difficult to estimate coherence at frequencies higher than 1/250 years.

[32] Low frequency changes in 79GGC $\delta^{18}O$ lead those in 8GGC by 30–50 years (Figure 5e). This could be a function of either age model error or different depth habitats for *G. ruber* and *G. sacculifer*. Each age model has ^{14}C tie point uncertainty due to analytical error (average ~50 years; Table 1), unknown changes in ^{14}C reservoir age, and bioturbation of foraminifera from adjacent depths. Ages between tie points have additional uncertainty due to variable sedimentation rate. While any one of these factors could account for a 50 year difference in the timing of similar $\delta^{18}O$ excursions in the two cores, it seems unlikely that age model uncertainty would produce a consistent offset across multiple frequencies. If *G. sacculifer* secretes more of its calcite in deeper, older water than *G. ruber* [*Duplessy et al.*, 1981], then the predominantly *G. sacculifer*-based age model for 79GGC would tend to be older than the 8GGC age model, similar to the phase relationship we observe (Figure 4e).

6. Discussion

6.1. Regional Ocean Dynamics

[33] A key question is whether the variability in the $\delta^{18}O$ records is representative of the Florida Current as a whole or due to the regional behavior of the Loop Current (LC) and Tortugas eddy system. Today, sea surface temperature at the core locations decreases due to the episodic formation of Tortugas eddies, which occur when the LC penetrates into the eastern Gulf of Mexico. When the LC retreats, water flows directly from the Yucatan Channel to the Straits of Florida, and Tortugas eddies fail to materialize (*Lee et al.* [1995]; see also http://e450.colorado.edu/realtime/gom_overlay/). As a result, the axis of the Florida Current shifts northward, and SST at the core sites increases (see http://fermi.jhuapl.edu/avhrr/gm/averages/index.html).

[34] While we cannot rule out that long-term shifts in the frequency of Tortugas eddy formation influenced our $\delta^{18}O$ records, instrumental data imply this process is an instability in the LC-Florida Current system unrelated to any obvious climate forcing. Northward penetration of the LC, a precursor to Tortugas eddy formation, lacks a clear seasonal signal and appears to be unrelated to Florida Current transport [*Maul and Vukovich*, 1993]. The shedding of anticyclonic rings from the LC, which occurs when the LC is well developed, also seems to be aperiodic [*Vukovich*, 1988; *Sturges and Leben*, 2000]. Potential vorticity flux through the Yucatan Channel may be an important control on LC development [*Candela et al.*, 2002], but it is unclear how climate variability would affect this flux. If Tortugas eddy formation is sensitive to changes in climate, our time series would indicate greater frequency of eddy formation, and

Figure 4. (a) Multitaper spectra for 79GGC. We calculated the spectrum for the 79GGC time series using two different age models, one using linear interpolation (dark line), and the other spline-based interpolation (gray line). In each case we used five discrete prolate spheroidal (Slepian) sequences with a time bandwidth product of 3 to window the data. For the linear age model, there are concentrations of power at periods 360, 190, 130, 100, and 80 years. The spline model yields different results, with the peaks near 360, 90, and 50 years. Confidence intervals are given by the vertical bars. (b) Multitaper spectra for 79GGC, 0–2850 years. The spectrum for each age model option indicates power near 1/125 years, significantly different than the spectra based on the longer time series. For the linear model, there is a broad spectral peak centered at 1/500 years. (c) Multitaper spectra for 8GGC. Only the linear age model yielded a significant peak, at 130 years. (d) Coherence for 79GGC and 8GGC (black curve, linear age model; gray curve, spline age model). Coherence was estimated using the multitaper window method with 15 windows and a time bandwidth product of 8. The MATLAB code used to estimate coherence and phase was provided by P. Huybers (http://web.mit.edu/~phuybers/www/Mfiles/index.html). The zero coherence level (horizontal dashed line; 95% confidence) indicates the two cores are coherent at frequencies lower than ~1/250 years. The lack of coherence at higher frequencies is likely a result of age model uncertainty. (e) Phase estimate for 79GGC and 8GGC. Across the low frequencies, 79GGC consistently leads 8GGC by 30–50 years. This offset is most likely related to the different foraminiferal species used for radiocarbon analyses to develop each age model (see text for details). Uncertainty in the phase estimate was determined using a Monte Carlo-based approach. The 95% and 80% confidence intervals are represented by the light gray and dark gray areas, respectively.

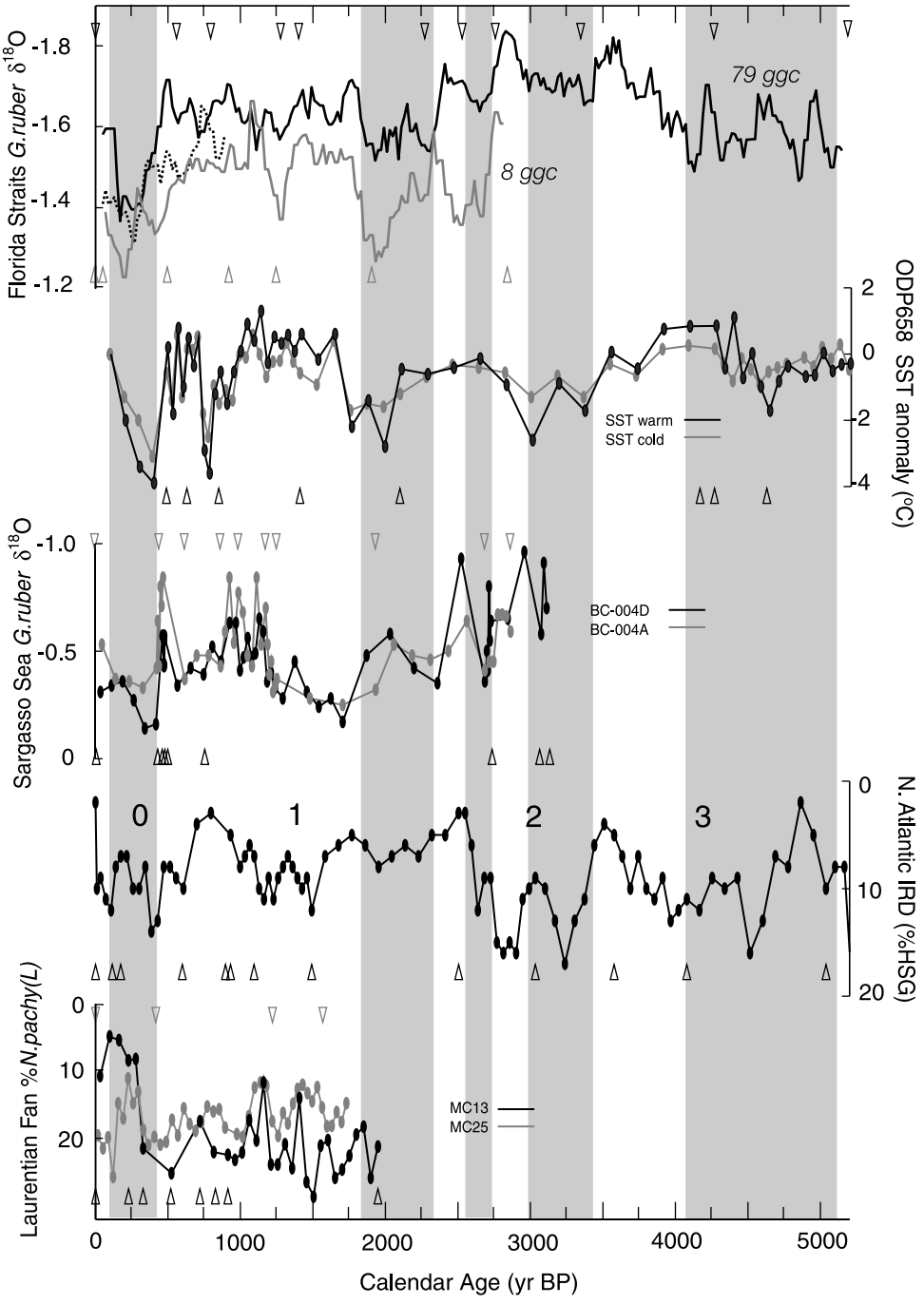

Figure 5. Comparison of the Florida Current $\delta^{18}O$ time series to paleoceanographic records from off the coast of west Africa (Site 658C; *deMenocal et al.* [2000]), the Sargasso Sea [*Keigwin*, 1996], the subpolar North Atlantic [*Bond et al.*, 2001], and south of Newfoundland [*Keigwin and Pickart*, 1999]. The vertical gray bars indicate intervals of generally heavy $\delta^{18}O$ in the Florida Current. Calendar ages for each time series are denoted with triangles. During the LIA, heavy $\delta^{18}O$ in 79GGC, 8GGC, and 62MC corresponds to enriched ^{18}O in the Sargasso Sea, SST cooling at Site 658C, increased ice-rafted debris (IRD) in the subpolar North Atlantic, and apparent warming (low % *N. pachyderma* (s.)) south of Newfoundland. The relative timing of earlier events is less clear, although high $\delta^{18}O$ in the Florida Straits generally corresponds to negative SST anomalies off the coast of west Africa.

presumably LC penetration, during intervals of high $\delta^{18}O$. Given the apparently stochastic nature of Tortugas eddy formation, however, we assume that their presence has little effect on mean Florida Current $\delta^{18}O$ on centennial and longer timescales.

6.2. North Atlantic Subtropical Gyre

[35] The $\delta^{18}O$ time series indicate the surface waters of the Florida Straits were cooler and/or more saline from approximately 50 to 400 cal years BP compared to today. This interval coincides very closely to the timing of the Little Ice Age observed in a variety of historical and paleoclimatic records. Similarly, a relatively warm and/or less saline interval from 450 to 1800 cal years BP encompasses the Medieval Warm Period. Several paleoceanographic records in the North Atlantic subtropical gyre are consistent with an SST cooling during the Little Ice Age (Figure 5). High $\delta^{18}O$ in the Florida Margin cores coincides with high $\delta^{18}O$ in the northwestern Sargasso Sea [*Keigwin*, 1996] and faunal-based estimates of SST cooling off the coast of west Africa (Site 658C; *deMenocal et al.* [2000]). At each of these three locations, there is a prominent event that began at approximately 400 years BP. The precise timing is difficult to constrain given age model uncertainty, but the apparent cooling is synchronous within chronological error at these three sites. Preceding this event at the coastal west Africa and Sargasso Sea sites is a similar but smaller amplitude cooling that began around 1000 A.D. This two-stage character of the LIA is not apparent in the Florida margin cores.

[36] At about 1000 years BP, surface water at the three subtropical gyre locations were apparently warmer or less saline than during the Little Ice Age. Prior to 1200 years BP, however, the records are quite different; in the Sargasso Sea, there is an interval of low $\delta^{18}O$ between 1200 and 800 years BP, while low $\delta^{18}O$ at the Florida Margin sites occurs from 1800 to 700 years BP, also an interval of warm SSTs off the coast of west Africa. To make the Sargasso Sea record consistent would require an age model adjustment of approximately 600 years in this interval; either the two Florida margin gravity cores and Site 658 are 600 years too old, the two Sargasso Sea box subcores are 600 years too young, or some combination of the two. This degree of age offset is unlikely to be caused by chronological errors, so it seems likely that the interval of low density in the Florida Current and high SST anomalies off the coast of west Africa began before the apparent warming in the Sargasso Sea.

[37] The timing of events in the subtropical gyre prior to the MWP is less clear, but overall it appears there were similar changes at each site. Intervals of high $\delta^{18}O$ centered at ~2000, 3200, and prior to 4000 cal years BP in the Florida Straits appear to be contemporary with cool SST events off the coast of west Africa (Figure 5). The two intervals of low $\delta^{18}O$ at 2400 and 2800 cal years BP in 79GGC are within dating error of similar excursions in the Sargasso Sea. Low $\delta^{18}O$ in 79GGC at ~2400 and 2800 cal years BP may coincide with the broad warming in site 658C from 2000 to 2800 cal years BP, but site 658C lacks two distinct events. Spectral analysis of site 658C and 79GGC show no significant coherent behavior if the full 5200-year 79GGC record is used, but the two sites are coherent at low frequencies (>1/300 years) if the analysis is limited to the 0–2000 years BP time span. The Sargasso Sea and 79GGC records are coherent between frequencies of ~1/1000 and 1/250 years for the common interval of 0 to 3000 years BP.

6.3. Subpolar North Atlantic

[38] The scope of the middle to late Holocene climate variability extends beyond the subtropical gyre into the subpolar North Atlantic. Marine sedimentary records of ice-rafted debris (IRD) imply that colder, ice-bearing waters episodically advected to the south and east of source regions in the Labrador and Nordic Seas [*Bond et al.*, 2001]. During the LIA, when the age control is robust, low apparent SSTs in the subtropical gyre correspond to IRD event 0, but there is no clear pattern for earlier events (Figure 5). IRD event 1 matches an interval of high $\delta^{18}O$ in the Sargasso Sea but it corresponds to warm SSTs at Site 658C and low $\delta^{18}O$ in the Florida Straits. IRD events 2 and 3 (at about 3000 years BP and 4500 years BP, respectively) overlap with intervals of both low and high $\delta^{18}O$ in the Florida Current. Asynchronous changes in the time domain are consistent with the lack of statistical coherence between Florida Straits $\delta^{18}O$ and subpolar North Atlantic IRD across all frequencies. At this stage it is difficult to determine whether the discrepancies between these records are real and reflect complex ocean-atmosphere dynamics, or an artifact of the age models and proxies used.

6.4. External Forcing

[39] Owing to the correlation of solar and climatic proxies at several sites, variability in late Holocene climate has been attributed in part to variations in solar forcing. Using a simple energy balance model, *Crowley* [2000] found that solar forcing accounts for a maximum of 31% of the temperature variance in the *Mann et al.* [1999] reconstruction from A.D. 1000–1850. Low solar activity inferred from low sunspot numbers during the Maunder Minimum (~1650–1710 A.D.) corresponds to high levels of atmospheric radiocarbon [*Eddy*, 1976], and cold Northern Hemisphere temperatures [*Bradley and Jones*, 1993]. It is estimated that solar irradiance was ~0.25% lower than today during the Maunder Minimum [*Lean et al.*, 1992].

[40] *Rind and Overpeck* [1993] simulated the climatic consequences of a 0.25% reduction in solar irradiance using an atmospheric general circulation model (AGCM). The model results produced a global annual average cooling of ~0.5°C, but the change in surface temperatures was spatially heterogeneous. The greatest cooling occurred over the continents (−1°C), while moderate warming occurred in and to the southeast of the Labrador Sea (+0.5°C). *Shindell et al.* [2001] found similar patterns using an updated AGCM that includes parameterizations of stratospheric ozone response to solar irradiance. Changes in oceanic circulation not included in these simulations may significantly alter the modeled SST patterns.

[41] The spatially variable temperature response of the models to decreased insolation is similar to that observed during the Little Ice Age. While temperatures in the Florida

Current, Sargasso Sea, and off the coast of west Africa all seemed to decrease, SSTs south of Newfoundland increased [*Keigwin and Pickart*, 1999]. The decrease in solar irradiance is also consistent with historical records of continental cooling during the LIA [*Grove*, 1988; *Jones and Bradley*, 1995] and borehole temperature evidence for a cold LIA in Greenland [*Dahl-Jensen et al.*, 1998]. *Shindell et al.* [2001] attributed the regional temperature pattern in their simulation to a shift in climatic conditions toward the low state of the Arctic Oscillation (or negative phase of the North Atlantic Oscillation (NAO)), where onshore flow of warm oceanic air is reduced during winter, generally resulting in cooler continents and warmer oceans in the circum-North Atlantic region. One exception to this pattern is the western subtropical North Atlantic, which cools during the NAO negative phase [*Walter and Graf*, 2002].

[42] If solar forcing played a dominant role in Holocene climate variability, we should find evidence of its influence in Florida Current $\delta^{18}O$. The spectrum for 79GGC has a concentration of power near 1/190 years (Figure 4a) and atmospheric $\Delta^{14}C$ has a well-known spectral peak at 1/200 years (Figure 6a; *Stuiver et al.* [1991]). In addition to 79GGC there are several late Holocene records from the Caribbean/Gulf of Mexico region that exhibit centennial-scale variability. A dominant period of ~200 years in Yucatan Peninsula drought records appears to be coherent with atmospheric $\Delta^{14}C$ [*Hodell et al.*, 2001]. Multiple centennial-scale features also appear in *G. sacculifer* abundance data from the Gulf of Mexico [*Poore et al.*, 2003] and *G. bulloides* abundance data from the Cariaco Basin [*Peterson et al.*, 1991].

[43] Although it is tempting to link Florida Current $\delta^{18}O$ and atmospheric $\Delta^{14}C$ because of their common spectral peak near 1/200 years, the two records are not coherent at this frequency (Figure 6b). Florida Current $\delta^{18}O$ and $\Delta^{14}C_{atm}$ are coherent near 1/100 and 1/50 years, but only if the linear interpolation age model for 79GGC is used. The two records may in fact be coherent in this part of the spectrum, but as is the case with 79GGC and 8GGC (Figure 4d), it appears that $\delta^{18}O$ signal noise and age model error preclude reliable coherence estimates at frequencies higher than 1/250 years. While Florida Current $\delta^{18}O$ and $\Delta^{14}C_{atm}$ lack coherence at timescales typically associated with solar variability, the two records are coherent at frequencies lower than ~1/300 years (Figure 6b). In general, $\delta^{18}O$ and $\Delta^{14}C_{atm}$ are in phase, although uncertainty in the estimate ranges from 10 to 50 degrees in the low frequencies (Figure 6c).

[44] The 79GGC $\delta^{18}O$ spectrum is also coherent at low frequencies with an estimate of Holocene ^{14}C production rate ($^{14}C_{pr}$). *Bond et al.* [2001] used a simple geochemical box model to simulate production rate changes necessary to yield the observed $\Delta^{14}C_{atm}$ signal. Although the $^{14}C_{pr}$ spectrum has a peak near 1/200 years (Figure 6d), it has less power at low frequencies than the linearly detrended $\Delta^{14}C_{atm}$ record (Figure 6a). Florida Current $\delta^{18}O$ and $^{14}C_{pr}$ are coherent at periods between ~300 and 1000 years (Figure 6e), but lack coherence at longer periods. While it appears that changes in $^{14}C_{pr}$ generally lead $\delta^{18}O$ (Figure 6f), the large error in the phase estimate makes it difficult to determine true leads or lags between the two time series.

[45] What climatic mechanism might cause surface density of the Florida Current and atmospheric $^{14}C_{pr}$ to vary together over centennial timescales? One possibility is that low solar irradiance caused ^{14}C production to increase and the surface ocean to cool. *Bond et al.* [2001] argued that centennial-scale increases in ice-rafted debris in the North Atlantic were coherent with high ^{14}C production rate and ice core ^{10}Be, or low apparent solar activity. On the basis of this correlation, the authors concluded that intervals of decreased solar irradiance during the past 12,000 years caused ice-bearing waters from the Labrador and Nordic Seas to more frequently advect to core sites in the northeast Atlantic.

[46] Atmospheric general circulation model results imply that parts of the North Atlantic subtropical gyre may have cooled by up to 1°C during the Maunder Minimum due to a solar irradiance-driven shift toward the NAO negative phase [*Shindell et al.*, 2001]. Although the simulated cooling in the Florida Straits is small (<0.2°C), changes in ocean circulation (which were not included in the AGCM) may have further amplified the cooling signal. Therefore in the frequency band of 1/1000 to 1/300 years, low solar activity (high $^{14}C_{pr}$) could lead to cooling in the Florida Straits and an increase in *G. ruber* $\delta^{18}O$.

6.5. Internal Forcing

[47] Internal climate system dynamics may act independently of solar activity to create Late Holocene climate variability. A prolonged negative phase of the North Atlantic Oscillation (NAO) has been invoked to explain cool SSTs in the Sargasso Sea and warm SSTs south of Newfoundland during the Little Ice Age (Figure 5) [*Keigwin and Pickart*, 1999]. On interannual timescales the negative phase of the NAO is characterized by warming in Greenland and off the coast of west Africa, however, patterns not observed during the LIA [*deMenocal et al.*, 2000]. Yet evaluating centennial-scale climate variability using the analogy of interannual NAO patterns may be misleading. If the climate system is forced toward one state of the NAO for decades or longer, the thermal inertia of the ocean and ocean-atmosphere feedbacks could create significantly different temperature anomalies. For instance, on multidecadal timescales the positive phase of the NAO is associated with warming in the subpolar gyre and cooling in the western subtropical Atlantic, opposite the interannual pattern [*Visbeck et al.*, 2003]. This is apparently due to either increased oceanic meridional overturning or advection of warm SST anomalies from the western subtropical Atlantic [*Visbeck et al.*, 2003]. Therefore, if we were to use decadal-scale NAO patterns from observational data as an analogy for the Little Ice Age, the SST pattern during the LIA (warming south of Newfoundland and apparent cooling in the Florida Straits, Sargasso Sea, and off the coast of west Africa) would actually imply a shift toward the NAO positive phase.

[48] Changes in the frequency and magnitude of the El Niño Southern Oscillation may also contribute to Late Holocene climate variability. Coral $\delta^{18}O$ records show a

decreased zonal SST gradient in the equatorial Pacific during the Little Ice Age, possibly related to more frequent El Niño events during this time [*Hendy et al.*, 2002; *Cobb et al.*, 2003]. High-resolution terrestrial rainfall records from both the Yucatan Peninsula and the Cariaco Basin indicate the Little Ice Age represents unusually dry conditions in these two regions. Gastropod $\delta^{18}O$ in lake sediments from the Yucatan Peninsula reveal a greater prevalence of drought during the LIA [*Hodell et al.*, 2001, 2002], consistent with evidence for increased aridity inferred from trace

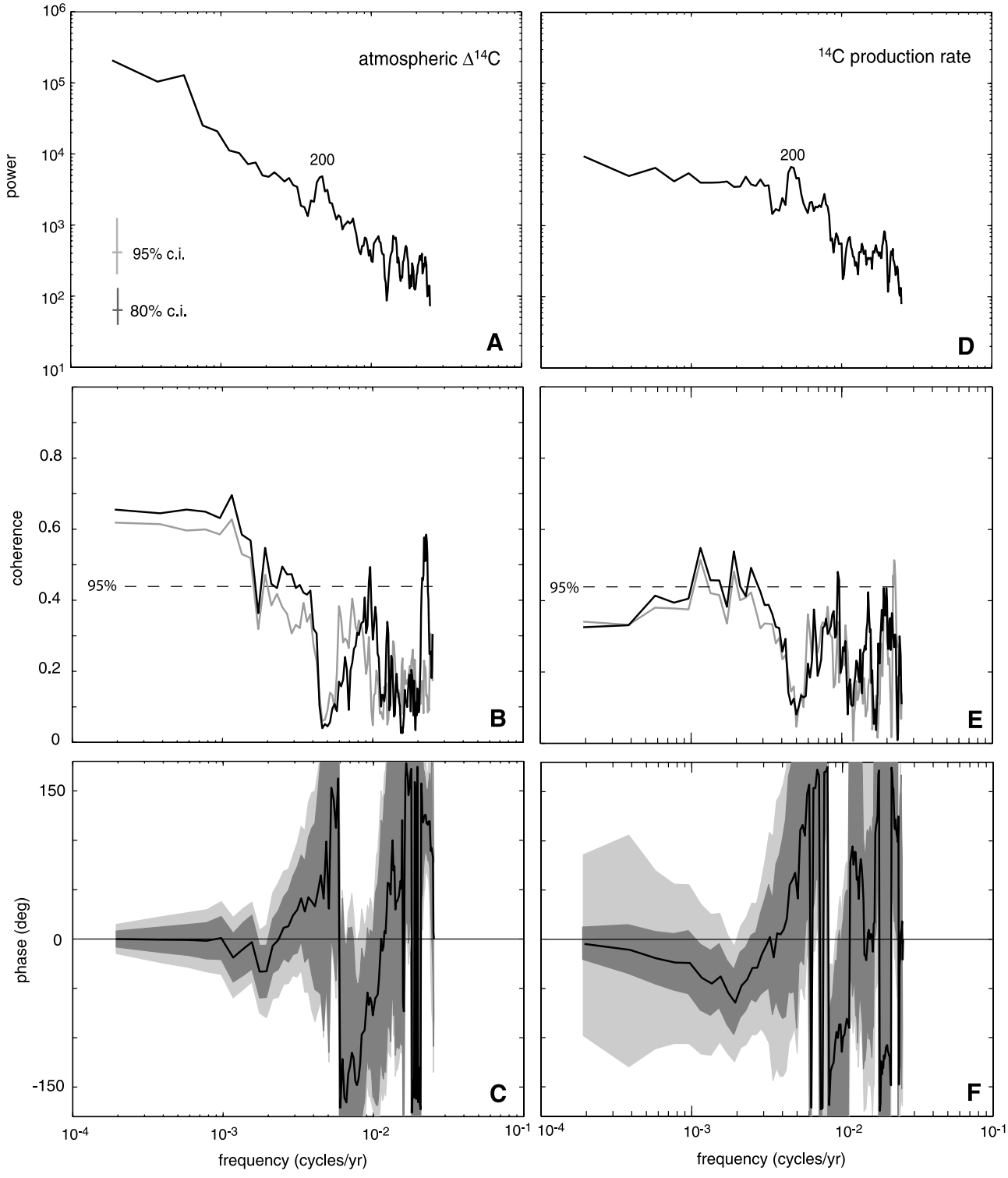

Figure 6

metals in the Cariaco Basin [*Haug et al.*, 2001]. In both cases, the rainfall records imply a southward shift of the intertropical convergence zone (ITCZ) during the LIA, perhaps as a result of a greater meridional temperature gradient in the North Atlantic or El Niño-like conditions in the equatorial Pacific [*Haug et al.*, 2001].

[49] If the Intertropical Convergence Zone shifted southward during the Little Ice Age, it could potentially increase the salinity of Florida Current (FC) surface waters. *Black et al.* [2004] invoke this mechanism as one possible explanation of the increase in Cariaco Basin planktonic $\delta^{18}O$ over the past 2000 years. Given that FC surface water is primarily south and equatorial Atlantic in origin [*Schmitz and Richardson*, 1991], it is not clear that a southward shift in ITCZ position would have a significant influence on FC surface salinity. If evaporation and precipitation patterns were similar to today during the LIA, then decreased Gulf Stream transport, and hence less export of salt from the subtropical gyre, could lead to more saline conditions in the Florida Current.

[50] A reduction in the cross-equatorial flow of warm surface waters which compensate North Atlantic Deep Water (NADW) would likely increase the North Atlantic SST gradient. Model simulations of strongly reduced NADW formation yield large meridional SST gradients in the North Atlantic and widespread cooling throughout the region [e.g., *Manabe and Stouffer*, 1988; *Schiller et al.*, 1997]. There is little direct evidence for a change in deep water production during the LIA, however. Benthic $\delta^{13}C$ data from the Bermuda Rise imply a decrease in the relative contribution of northern source deep waters during the Little Ice Age, but Cd/Ca analyses from the same cores show relatively little change [*Keigwin and Boyle*, 2000]. *Bianchi and McCave* [1999] suggest that sedimentary grain size evidence implies a reduction in Iceland-Scotland Overflow Water during the LIA. Benthic $\delta^{13}C$ data from the subpolar northeastern Atlantic are consistent with reduced NADW flow during some intervals of high ice rafting, implying meridional overturning may vary on millennial timescales during the Holocene [*Oppo et al.*, 2003], but this record ends prior to the LIA.

[51] The coherent and in-phase relationship between the detrended atmospheric $\Delta^{14}C$ and Florida Current $\delta^{18}O$ records at periods >1000 years (Figure 6b) raises the possibility that oceanic circulation influences the behavior of ^{14}C on millennial timescales. The relatively low coherence between ^{14}C production rate and $\delta^{18}O$ at these frequencies (Figure 6e) further implies that solar variability is not a likely driver of the $\delta^{18}O$ signal on longer timescales. Reduced meridional overturning circulation (MOC) may have caused both low SSTs in the subtropical gyre and less sequestration of radiocarbon in the deep ocean (higher $\Delta^{14}C_{atm}$). Model simulations of a shutdown of North Atlantic Deep Water yield SST cooling of $\sim$1°C in the western subtropical gyre [*Manabe and Stouffer*, 1988; *Schiller et al.*, 1997]. While this could account for $\delta^{18}O$ changes in the Florida Current and Sargasso Sea during the LIA, there is no evidence in support of a NADW shutdown at this time. It is possible that the models lack adequate sensitivity to MOC variability or additional mechanisms such as the NAO play a role in amplifying the SST response.

[52] The idea that oceanic circulation had a significant influence on atmospheric $\Delta^{14}C$ during the Holocene is usually discredited due to the similarity of ^{14}C and ^{10}Be records at centennial timescales. *Beer et al.* [1988] simulated atmospheric $\Delta^{14}C$ using the concentration of ^{10}Be in the Camp Century ice core as a proxy for cosmogenic nuclide production. At frequencies higher than 1/1000 years, modeled and observed $\Delta^{14}C$ share approximately 36% of their variance during the late Holocene [*Beer et al.*, 1988]. A similar degree of shared variance is found between bandpass filtered records of modeled ^{14}C production rate and ^{10}Be flux from the GRIP and GISPII ice cores [*Bond et al.*, 2001]. *Bard et al.* [2000] were able to closely model the detrended record of atmospheric $\Delta^{14}C$ for the past 1200 years using a ^{10}Be-based estimate of cosmogenic nuclide production from the South Pole. Since ^{14}C and ^{10}Be have different life histories, similar variability in each are most easily attributed to changes in production rate.

[53] On millennial timescales it is less clear that solar variability plays an important role in controlling atmospheric $\Delta^{14}C$. The long-term decrease in Holocene atmospheric $\Delta^{14}C$ is most likely due to increasing strength in the geomagnetic dipole, but offsets of ±20‰ between observed and geomagnetically driven changes in $\Delta^{14}C$ remain unex-

Figure 6. (a) Multitaper spectrum for atmospheric $\Delta^{14}C$, 0–5200 years BP, linearly detrended and sampled at 20-year intervals. The well-documented spectral peak near 1/200 years is apparent. Confidence intervals are given by the vertical bars (95%, gray; 80%, black). (b) Multitaper coherence for 79GGC and atmospheric $\Delta^{14}C$, 0–5200 years BP. Estimates for the 79GGC linear (black) and spline (gray) age model both indicate coherence at frequencies lower than 1/300 years. The linear model also has coherent features at higher frequencies, near 1/100 and 1/45 years, but these are lacking from the spline-based estimate. The 95% confidence limit is given by the horizontal dashed line. (c) Phase for 79GGC and atmospheric $\Delta^{14}C$. At low frequencies the records appear to be in phase. The 95% and 85% confidence limits, based on Monte Carlo simulations, are indicated by the light and dark gray areas, respectively. A similar phase relationship exists for the spline age model (not shown). Both coherence and phase were estimated using the MATLAB routine provided by P. Huybers. (d) Same as Figure 6a, except using the ^{14}C production rate time series from *Bond et al.* [2001]. The spectrum also has significant power at 1/200 years but lacks the low-frequency power of $\Delta^{14}C$. (e) Multitaper coherence for 79GGC $\delta^{18}O$ and ^{14}C production rate 0–5200 years BP. Florida Current $\delta^{18}O$ and ^{14}C production rate are coherent at frequencies between $\sim$1/1000 and 1/300 years but lack the lower frequency coherence apparent with $\Delta^{14}C$. (f) Phase for 79GGC $\delta^{18}O$ and radiocarbon production rate. At coherent frequencies, production rate leads $\delta^{18}O$, but only at the 80% confidence level.

plained [*Stuiver et al.*, 1991]. The $\Delta^{14}C$ offsets could be a function of undocumented millennial-scale solar variability, uncertainties in the geomagnetic reconstruction, or changes in the partitioning of carbon between the ocean, atmosphere, and terrestrial biosphere. While the data presented here are far too limited to choose between these possibilities, the coherence of Florida Current $\delta^{18}O$ and atmospheric $\Delta^{14}C$ at millennial timescales is consistent with an oceanic contribution.

7. Conclusion

[54] Planktonic foraminiferal oxygen isotopes indicate that the Florida Current was cooler or more saline during the Little Ice Age than today, and was relatively warm or fresh during the Medieval Warm Period. Much of the North Atlantic subtropical gyre responded in a similar manner. Given that the El Niño Southern Oscillation has little direct effect on SSTs in this region (see http://www.cdc.noaa.gov/ENSO/), it is unlikely that ENSO on its own was responsible for the gyre-wide hydrographic changes. A more feasible option is long-term changes in the behavior of the North Atlantic Oscillation. Results from an atmospheric general circulation model imply that low solar irradiance during the LIA may have triggered a shift toward the NAO negative phase, resulting in a cool subtropical gyre and warm subpolar gyre, similar to the observed pattern [*Shindell et al.*, 2001]. Alternatively, instrumental data indicate that on decadal and longer timescales, cool SST anomalies in the subtropical gyre and warm SST anomalies in the subpolar gyre are associated with the positive phase of the NAO [*Visbeck et al.*, 2003]. This pattern is apparently caused by oceanic advection of warm anomalies from the western subtropical Atlantic or enhanced meridional overturning circulation [*Visbeck et al.*, 2003].

[55] The coherence and phasing of atmospheric ^{14}C production and Florida Current $\delta^{18}O$ during the Late Holocene implies that solar variability may influence FC surface density at frequencies between 1/300 and 1/1000 years. *Bond et al.* [2001] argue that a solar mechanism can account for the similarity between proxies of solar variability and ice-rafting in the subpolar North Atlantic. Solar irradiance-driven changes in surface temperature modeled by *Shindell et al.* [2001] underestimate the observed cooling in Greenland and the North Atlantic subtropical gyre by 1°C or more. Either model sensitivity to solar irradiance is too low, another mechanism is required to amplify the temperature response, or the subtropical gyre records reflect changes in salinity rather than temperature.

[56] One plausible option is that variability internal to the climate system influences Florida Current $\delta^{18}O$, ice-rafting in the North Atlantic and atmospheric $\Delta^{14}C$. Ocean general circulation models indicate the entire North Atlantic cools during severe reductions in NADW formation. Yet it seems unlikely that a change in NADW formation on its own caused the LIA cooling, given the warming south of Newfoundland at this time [*Keigwin and Pickart*, 1999]. If meridional overturning episodically slowed during the Late Holocene, it should lead to a cooling of the subtropical gyre, consistent with the pattern during the LIA. Reduced overturning would in turn limit sequestration of ^{14}C in the deep sea, and therefore cause an accumulation of ^{14}C in the atmosphere. The coherence between Florida Current $\delta^{18}O$ and atmospheric $\Delta^{14}C$ at periods greater than 1000 years implies that internal climate system variability may influence the low-frequency behavior of atmospheric radiocarbon during the Late Holocene.

[57] **Acknowledgments.** We would like to thank Olivier Marchal, Jean Lynch-Stieglitz, and two anonymous reviewers for their valuable comments and suggestions. We also thank Peter Huybers for use of his multitaper coherence routine and Dorinda Ostermann, Marti Jeglinski, Anne Edwards, and Shawn Johnson for technical support. We are grateful to the WHOI core lab for sample collection and archiving, the captain and crew of the R/V *Knorr*, and to the Sea Education Association for access to their vessels *Westward* and *Cramer.* This work was supported by NSF grants OCE-9905605 and OCE-0096469. This is WHOI contribution 11236.

References

Bard, E., G. Raisbeck, F. Yiou, and J. Jouzel (2000), Solar irradiance during the last 1200 years based on cosmogenic nuclides, *Tellus, Ser. B*, *52*, 985–992.

Baringer, M. O., and J. C. Larsen (2001), Sixteen years of Florida Current transport at 27°N, *Geophys. Res. Lett.*, *28*, 3179–3182.

Beer, J. U. Siegenthaler, G. Bonami, R. C. Finkel, H. Oeschger, M. Suter, and W. Wölfli (1988), Information on past solar activity and geomagnetism from 10Be in the Camp Century ice core, *Nature*, *331*, 675–679.

Bianchi, G., and I. N. McCave (1999), Holocene periodicity in North Atlantic climate and deep-ocean flow south of Iceland, *Nature*, *397*, 515–517.

Black, D. E., R. C. Thunell, A. Kaplan, L. C. Peterson, and E. J. Tappa (2004), A 2000-year record of Caribbean and tropical North Atlantic hydrographic variability, *Paleoceanography*, *19*, PA2022, doi:10.1029/2003PA000982.

Bond, G., B. Kromer, J. Beer, R. Muscheler, M. N. Evans, W. Showers, S. Hoffmann, R. Lotti-Bond, I. Hajdas, and G. Bonami (2001), Persistent solar influence on North Atlantic climate during the Holocene, *Science*, *294, 2130–2136.*

Bradley, R. S., and P. D. Jones (1993), Little Ice Age summer temperature variations: their nature and relevance to recent global warming trends, *Holocene*, *3*, 367–376.

Candela, J., J. Sheinbaum, J. Ochoa, and A. Badan (2002), The potential vorticity flux through the Yucatan Channel and the Loop Current in the Gulf of Mexico, *Geophys. Res. Lett.*, *29*(22), 2059, doi:10.1029/2002GL015587.

Chinn, T. J. (1996), New Zealand glacier responses to climate change of the past century, *N. Z. J. Geol. Geophys.*, *39*, 415–428.

Cobb, K. M., C. D. Charles, H. Cheng, and R. L. Edwards (2003), El Niño/Southern Oscillation and tropical Pacific climate during the last millennium, *Nature*, *424*, 271–276.

Crowley, T. J. (2000), Causes of climate change over the past 1000 years, *Science*, *289*, 270–277.

Curry, W. B., R. C. Thunell, and S. Honjo (1983), Seasonal changes in the isotopic composition of planktonic foraminifera collected in Panama Basin sediment traps, *Earth Planet. Sci. Lett.*, *64*, 33–43.

Dahl-Jensen, D., K. Mosegaard, N. Gundestrup, G. D. Clow, S. J. Johnsen, A. W. Hansen, and N. Balling (1998), Past temperatures directly from the Greenland ice sheet, *Science*, *282*, 268–271.

deMenocal, P., J. Ortiz, T. Guilderson, and M. Sarnthein (2000), Coherent high- and low-latitude variability during the Holocene warm period, *Science*, *288*, 2198–2202.

Denton, G. H., and W. Karlén (1973), Holocene climatic variations-their pattern and possible cause, *Quat. Res.*, *3*, 155–205.

Deuser, W. G. (1987), Seasonal variations in isotopic composition and deep-water fluxes of the tests of perennially abundant planktonic foraminifera of the Sargasso Sea: Results from sediment-trap collections and their paleoceanographic significance, *J. Foraminiferal Res.*, *17*, 14–27.

Druffel, E. M. (1982), Banded corals: Changes in oceanic carbon-14 during the Little Ice Age, *Science*, *218*, 13–19.

Duplessy, J. C., P. L. Blanc, and A. W. H. Bé (1981), Oxygen-18 enrichment of planktonic foraminifera due to gametogenic calcification below the euphotic zone, *Science*, *213*, 1247–1250.

Eddy, J. M. (1976), The Maunder Minimum, *Science*, *192*, 1189–1202.

Epstein, S., R. Buchsbaum, H. A. Lowenstam, and H. C. Urey (1953), Revised carbonate water isotopic temperature scale, *Geol. Soc. Am. Bull.*, *64*, 1315–1326.

Esper, J., E. R. Cook, and F. H. Shweingruber (2002), Low-frequency signals in long tree-ring chronologies for reconstructing past temperature variability, *Science*, *295*, 2250–2253.

Etheridge, D. M., L. P. Steele, R. L. Langenfelds, R. J. Francey, J. M. Barnola, and V. I. Morgan (1996), Natural and anthropogenic changes in atmospheric CO2 over the last 1000 years from air in Antarctica ice and firn, *J. Geophys. Res.*, *101*, 4115–4128.

Fairbanks, R. G., M. Sverdlove, R. Free, P. H. Wiebe, and Allan W. H. Bé (1982), Vertical distribution and isotopic fractionation of living planktonic foraminifera from the Panama Basin, *Nature*, *298*, 841–844.

Fairbanks, R. G., C. D. Charles, and J. D. Wright (1992), Origin of global meltwater pulses, in *Radiocarbon After Four Decades*, edited by R. E. Taylor et al., pp. 473–500, Springer-Verlag, New York.

Fratantoni, P. S., T. N. Lee, G. P. Podesta, and F. Muller-Karger (1998), The influence of Loop Current perturbations on the formation and evolution of Tortugas eddies in the southern Straits of Florida, *J. Geophys. Res.*, *103*, 24,759–24,779.

Ganachaud, A., and C. Wunsch (2000), Improved estimates of global ocean circulation, heat transport and mixing from hydrographic data, *Nature*, *408*, 453–457.

Grove, J. M. (1988), *The Little Ice Age*, 498 pp., Methuen, New York.

Haase-Schramm, A., F. Böhm, A. Eisenhauer, W. Dullo, M. M. Joachimski, B. Hansen, and J. Reitner (2003), Sr/Ca ratios and oxygen isotopes from sclerosponges: Temperature history of the Caribbean mixed layer and thermocline during the Little Ice Age, *Paleoceanography*, *18*(3), 1073, doi:10.1029/2002PA000830.

Haug, G., K. A. Hughen, D. M. Sigman, L. C. Peterson, and U. Rohl (2001), Southward migration of the ITCZ through the Holocene, *Science*, *293*, 1304–1308.

Hendy, E. J., M. K. Gagan, C. A. Alibert, M. T. McCulloch, J. M. Lough, and P. J. Isdale (2002), Abrupt decrease in tropical Pacific sea surface salinity at end of Little Ice Age, *Science*, *295*, 1511–1514.

Hodell, D. A., M. Brenner, J. H. Curtis, and T. Guilderson (2001), Solar forcing of drought frequency in the Maya lowlands, *Science*, *292*, 1367–1370.

Hodell, D. A., et al. (2002), The Little Ice Age in Mesoamerica, *Eos Trans. AGU*, *83*(47), Fall Meet. Suppl., Abstract PP61B-10.

Huang, S., H. N. Pollack, and P. Shen (2000), Temperature trends over the past five centuries reconstructed from borehole temperatures, *Nature*, *403*, 756–758.

Indermühle, A., et al. (1999), Holocene carbon-cycle dynamics based on CO_2 trapped in ice at Taylor Dome, *Antarctica, Nature*, *398*, 121–126.

Jones, P. D., and R. S. Bradley (1995), Climate variations over the last 500 years, in *Climate Since A.D. 1500*, edited by R. S. Bradley and P. D. Jones, pp. 649–665, Routledge, New York.

Keigwin, L. (1996), The Little Ice Age and Medieval Warm Period in the Sargasso Sea, *Science*, *274*, 1504–1508.

Keigwin, L., and E. A. Boyle (2000), Detecting Holocene changes in thermohaline circulation, *Proc. Natl. Acad. Sci. U.S.A.*, *97*, 1343–1346.

Keigwin, L., and R. S. Pickart (1999), Slope Water Current over the Laurentian Fan on interannual to millennial time scales, *Science*, *286*, 520–523.

Killingley, J. S., R. F. Johnson, and W. H. Berger (1981), Oxygen and carbon isotopes of individual shells of planktonic foraminifera from Ontong-Java Plateau, equatorial Pacific, *Palaeogeogr. Palaeoclimatol. Palaeoecol.*, *33*, 193–204.

Kim, S. T., and J. O'Neil (1997), Equilibrium and non-equilibrium oxygen isotope effects in synthetic carbonates, *Geochim. Cosmochim. Acta.*, *61*, 3461–3475.

Larsen, J. C. (1992), Transport and heat flux of the Florida Current at 27°N derived from cross-stream voltages and profiling data: Theory and observations, *Philos. Trans. R. Soc. London A*, *338*, 169–236.

Lean, J., and D. Rind (1999), Evaluating Sun-climate relationships since the Little Ice Age, *J. Atmos. Terr. Phys.*, *61*, 25–36.

Lean, J., A. Skumanich, and O. White (1992), Estimating the Sun's radiative output during the Maunder Minimum, *Geophys. Res. Lett.*, *19*, 1591–1594.

Lee, T. N., K. Leaman, E. Williams, T. Berger, and L. Atkinson (1995), Florida Current meanders and gyre formation in the southern Straits of Florida, *J. Geophys. Res.*, *100*, 8607–8620.

Levitus, S., R. Burgett, and T. P. Boyer (1994), *World Ocean Atlas*, U.S. Dept. of Comm., Washington, D.C.

Lynch-Stieglitz, J., W. B. Curry, and N. Slowey (1999), A geostrophic estimate for the Florida Current from the oxygen isotope composition of benthic foraminifera, *Paleoceanography*, *14*, 360–373.

Manabe, S., and R. J. Stouffer (1988), Two stable equilibria of a coupled ocean-atmosphere model, *J. Clim.*, *1*, 841–866.

Mann, M. E., R. S. Bradley, and M. K. Hughes (1999), Northern Hemisphere temperatures during the past millennium: Inferences, uncertainties, and limitations, *Geophys. Res. Lett.*, *26*, 759–762.

Maul, G., and F. M. Vukovich (1993), The relationship between variations in the Gulf of Mexico Loop Current and Straits of Florida volume transport, *J. Phys. Oceanogr.*, *23*, 785–796.

Oppo, D. W., J. F. McManus, and J. L. Cullen (2003), Deep water variability in the Holocene epoch, *Nature*, *422*, 277–278.

Ostermann, D. R., and W. B. Curry (2000), Calibration of stable isotopic data: An enriched $\delta^{18}O$ standard used for source gas mixing detection and correction, *Paleoceanography*, *15*, 353–360.

Peterson, L. C., J. T. Overpeck, N. G. Kipp, and J. Imbrie (1991), A high-resolution Late Quaternary upwelling record from the anoxic Cariaco Basin, Venezuela, *Paleoceanography*, *6*, 99–119.

Poore, R. Z., H. J. Dowsett, S. Verardo, and T. M. Quinn (2003), Millennial- to century-scale variability in Gulf of Mexico Holocene climate records, *Paleoceanography*, *18*(2), 1048, doi:10.1029/2002PA000868.

Rind, D., and J. Overpeck (1993), Hypothesized causes of decade- to century-scale climate variability: Climate model results, *Quat. Sci. Rev.*, *12*, 357–374.

Schiller, A., U. Mikolajewicz, and R. Voss (1997), The stability of the North Atlantic thermohaline circulation in a couple ocean-atmosphere general circulation model, *Clim. Dyn.*, *13*, 325–347.

Schmitz, W. J., and M. S. McCartney (1993), On the North Atlantic Circulation, *Rev. Geophys.*, *31*, 29–49.

Schmitz, W. J., and P. Richardson (1991), On the sources of the Florida Current, *Deep Sea Res.*, *38*, s379–s409.

Schmitz, W. J., J. R. Luyten, and R. W. Schmitt (1993), On the Florida Current T/S envelope, *Bull. Mar. Sci.*, *53*, 1048–1065.

Shindell, D. T., G. A. Schmidt, M. E. Mann, D. Rind, and A. Waple (2001), Solar forcing of regional climate during the Maunder Minimum, *Science*, *294*, 2149–2152.

Spero, H. J., J. Bijma, D. W. Lea, and B. E. Bemis (1997), Effect of seawater carbonate concentration on foraminiferal carbon and oxygen isotopes, *Nature*, *390*, 497–500.

Stuiver, M., T. F. Braziunas, B. Becker, and B. Kromer (1991), Climatic, solar, oceanic and geomagnetic influences on late-glacial and Holocene atmospheric $^{14}C/^{12}C$ change, *Quat. Res.*, *35*, 1–24.

Stuiver, M., P. J. Reimer, E. Bard, J. W. Beck, G. S. Burr, K. A. Hughen, B. Kromer, F. G. McCormac, J. V. D. Plicht, and M. Spurk (1998), INTCAL98 radiocarbon age calibration 24,000–0 cal BP, *Radiocarbon*, *40*, 1041–1083.

Sturges, W., and R. Leben (2000), Frequency of ring separations from the Loop Current in the Gulf of Mexico: A revised estimate, *J. Phys. Oceanogr.*, *30*, 1814–1819.

Thompson, L. G. (1995), Ice core evidence from Peru and China, in *Climate Since A.D. 1500*, edited by R. S. Bradley and P. D. Jones, pp. 517–548, Routledge, New York.

Thomson, D. J. (1982), Spectrum estimation and harmonic analysis, *Proc. IEEE*, *70*, 1055–1096.

Visbeck, M., E. P. Chassignet, R. G. Curry, T. L. Delworth, R. R. Dickson, and G. Krahmann (2003), The ocean's response to North Atlantic Oscillation variability, in *The North Atlantic Oscillation: Climate Significance and Environmental Impact*, *Geophys. Monogr. Ser.*, vol. 134, edited by J. W. Hurrell et al., pp. 113–145, AGU, Washington, D. C.

Vukovich, F. M. (1988), Loop Current boundary variations, *J. Geophys. Res.*, *93*, 15,585–15,591.

Walter, K., and H. F. Graf (2002), On the changing nature of the regional connection

between North Atlantic Oscillation and sea surface temperature, *J. Geophys. Res.*, *107*(D17), 4338, doi:10.1029/2001JD000850.

Watanabe, T., A. Winter, and T. Oba (2001), Seasonal changes in sea surface temperature and salinity during the Little Ice Age in the Caribbean Sea deduced from Mg/Ca and $^{18}O/^{16}O$ ratios in corals, *Mar. Geol.*, *173*, 21–35.

Williams, D. F., Allan W. H. Bé, and R. G. Fairbanks (1979), Seasonal oxygen isotopic variations in living planktonic foraminifera off Bermuda, *Science*, *206*, 447–449.

Winter, A., H. Ishioroshi, T. Watanabe, T. Oba, and J. Christy (2000), Caribbean sea surface temperatures: Two-to-three degrees cooler than present during the Little Ice Age, *Geophys. Res. Lett.*, *27*, 3365–3368.

Zeebe, R. E. (1999), An explanation of the effect of seawater carbonate concentration on foraminiferal oxygen isotopes, *Geochim. Cosmochim. Acta*, *63*, 2001–2007.

W. B. Curry, Department of Geology and Geophysics, Woods Hole Oceanographic Institution, Woods Hole, MA 02543, USA.

D. C. Lund, MIT/WHOI Joint Program in Oceanography, Woods Hole Oceanographic Institution, Wood Hole, MA 02543, USA. (dlund@whoi.edu)

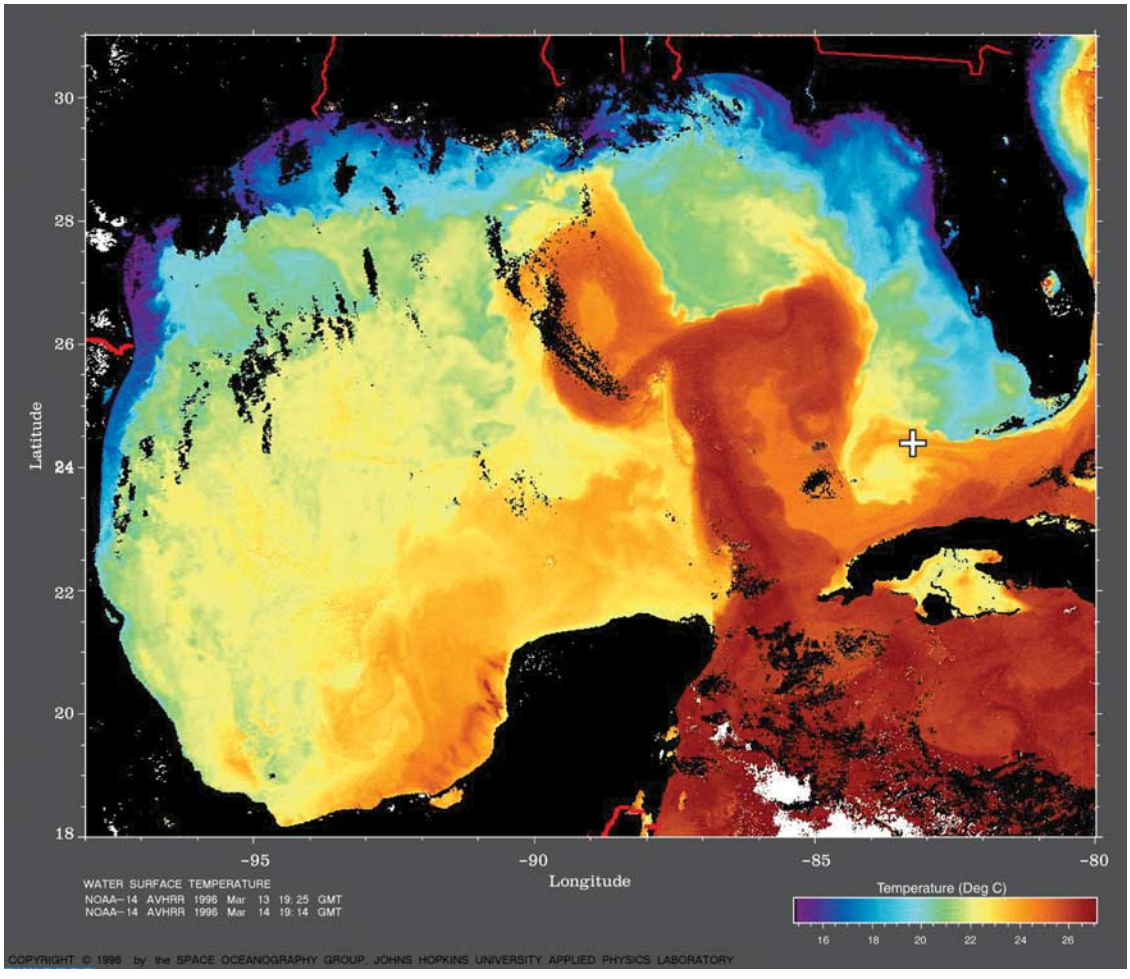

Figure 1. Advanced very high resolution radiometer (AVHRR)-based sea surface temperature estimates for the Gulf of Mexico and Florida Straits, 13–14 March 1996. SSTs in this figure vary from 15 to 27°C. The strong north-south temperature gradient near the core sites (plus symbol) is typical of winter conditions in this area (reprinted by permission from Ocean Remote Sensing Group, Johns Hopkins University Applied Physics Laboratory).